

# Non-imaging real-time detection and tracking of fast-moving objects using a single-pixel detector

Fengming Zhou<sup>a</sup>, Xuelei Shi<sup>b</sup>, Jie Chen<sup>b</sup>, Tianhang Tang<sup>b</sup>, and Yiguang Liu<sup>a,b,\*</sup>

<sup>a,b</sup>College of Computer Science, Sichuan University, Sichuan Province, 610065, China

**Abstract:** Real-time detecting and tracking of fast-moving object have achieved great success in speed and accuracy. However, available methods can hardly achieve real-time object detecting and tracking under low-cost conditions. To tackle this problem, a non-imaging strategy including two stages is proposed: 1) a sampling method, which is effective-area-optimized based on Hadamard single-pixel imaging technology, achieving ultra-low sampling, is adopted to optimize the Hadamard basis pattern sequence for reconstructing projection curves. The pattern is displayed by a spatial light modulator to illuminate a fast-moving object, while a single-pixel detector is used for data collection; 2) a non-imaging detection and tracking method is proposed to estimate fast-moving object location by calculating the gradient difference of the projection curves, which considers both sampling efficiency and location accuracy for real-time detecting and tracking. Experimental results have demonstrated that our method has good performance in real-time detection and tracking at 1.28% sampling rate and 105 fps frame rate. Combined with the wide-spectrum response capability of the single-pixel detector, our solution can achieve real-time detection and tracking of hidden fast-moving targets in invisible band.

**Keywords:** Hadamard basis pattern, single-pixel detector, gradient difference, tracking

## 1. Introduction

Real-time detection and tracking of fast-moving objects are widely used in scientific research, autonomous driving, industrial measurement, national defense security, bio-medicine and many other fields. Radar used for long-distance targets and large field of view is an image-free target detection and tracking technology [1-4]. It emits electromagnetic waves at a certain frequency. Electromagnetic waves are reflected when encountering an object and are detected by the radar when the radar does not emit electromagnetic waves, to achieve detection and tracking. With the development of various image sensors, compared with a radar system, the cost of image-based target detection and tracking system [5-7] is relatively low, and the application range is wider.

The detection and imaging are two independent parts of image-based moving object tracking method, that is, moving objects need to be detected and tracked from continuous and clear images, and its accuracy depends on the quality of the captured image. At this time, the main factor affecting the image quality is motion blur caused by fast-moving targets. To deal with motion blur, an imaging system and image processing algorithm with high time resolution are required. However, the equipment that constitutes a high time resolution imaging system is expensive, and the data throughput is usually very large in a short period of time, which requires a large data storage capacity and a wide data transmission bandwidth. And the advanced image processing and analysis algorithms will also take up a lot of computing resources. Gong W et al. [8-10] discussed high refresh rate and efficient reconstruction algorithms based on image moving target detection and tracking [11-15]. If the target is moving too fast, these methods are not applicable. Moreover, the

method of obtaining motion information through the evolution process of moving objects requires a high-precision tracking and aiming system [16-18]. Reference [19] proposed that target tracking does not require a clear image, and the position information of the target can be obtained from the relationship between the rough images of different positions of the target. However, this method also requires imaging with time and space costs. In summary, complex image processing and analysis algorithms and limited data processing capabilities have brought challenges to real-time target detection and tracking in practical applications.

In essence, the detection and tracking of fast-moving objects are to obtain their two-dimensional or three-dimensional spatial information, which has nothing to do with their own attributes. Compared with imaging that requires thousands of pixels, only two or three scalars are needed to determine the coordinates of the target, which reduces the amount of calculation by three to four orders of magnitude. As a result, in the image-based method, a large amount of captured image data brings huge time and space costs to the system. It goes without saying that the redundancy of data acquisition is one of the main reasons hindering real-time target detection and tracking. To solve this problem, Shi et al. [20] proposed a method based on single-pixel imaging, using the "slice theory" of Hadamard transform to decompose the Hadamard matrix, which can track the target without obtaining a complete image, but the scene background in this method is somewhat simple. And an imageless method was recently proposed, based on Fourier single-pixel imaging (SPI), which allows real-time tracking of fast-moving objects [21].

Here, a detection and tracking method that performs gradient difference calculation on the projection curves is proposed, named PCGD, which can realize real-time detection and tracking of fast-moving objects in a scene with complex backgrounds without imaging. Using the SPI-based technology [22-26], without acquiring the target scene image, reconstruct the projection curve of the complex scene in the x-axis and y-axis direction. And then calculate the gradient difference of the projection curve to obtain the position information of the fast-moving object. In other words, this means that the target scene is converted from two-dimensional to one-dimensional, reducing the amount of calculation and storage space occupation, and improving the calculation efficiency and real-time performance of the system strongly.

In addition, a new sampling method, which is effective-area-optimized based on Hadamard single-pixel imaging technology, named EAHSI, is adopted to improve the efficiency of reconstructing projection curves. It optimizes the Hadamard basis pattern sequence by selecting the projection order according to the size of the effective region where the energy can be concentrated in the pattern. Consequently, in the target detection and tracking method, a small number of patterns in the optimized sequence only need to be used to measure the signal required to reconstruct the projection curve, and then the light signal is collected by a single-pixel detector. Our method directly uses the single-pixel measurement values to reconstruct the projection curves, which can obtain the position information of the target without imaging. It has the ability of ultra-low sampling rate and high computational efficiency, which is suitable for the sampling stage of real-time detection and tracking of fast-moving objects.

## 2. Theory

### 2.1. Hadamard basis pattern construction and the principle of HSI

Hadamard single-pixel imaging (HSI) is an imaging technology based on the Hadamard transform [27-29]. HSI obtains the Hadamard spectrum of the image, and the image is reconstructed by inverse transformation. The Hadamard spectrum consists of a set of Hadamard coefficients, each corresponding to a unique pattern. Hadamard basis pattern, a standard orthogonal basis, is derived from Hadamard matrix, which a kind of square matrix whose elements are 1 and -1 and whose rows (or columns) are orthogonal to each other. Each Hadamard basis pattern is formed by reshaping a row (or a column) of the Hadamard matrix into a two-dimensional square, as illustrated in Fig. 2, and the lowest order Hadamard matrix is second-order:

$$H_2 = \begin{bmatrix} 1 & 1 \\ 1 & -1 \end{bmatrix}. \quad (1)$$

The Hadamard matrix of higher order is obtained by formula  $H_{2^{n+1}} = H_{2^n} \otimes H_2$ ,  $\otimes$  is a Kronecker product operator. The Hadamard coefficient can be obtained by projecting the pattern onto object, which is mathematically equivalent to the inner product between the Hadamard basis pattern and object. Therefore, the Hadamard spectrum can be reconstructed based on single-pixel measurement values.

When calculating the Hadamard spectrum, we employ differential HSI to suppress noise and each Hadamard coefficient  $H(u, v)$  to be obtained by differential computation [30-31]. Each illumination mode of the differential HSI has two measurement values, one measurement value is obtained by projecting pattern  $P_H(x, y)$  and the other is obtained by projecting pattern  $1 - P_H(x, y)$ , as shown in Fig. 1. The coefficient  $H(u, v)$  is obtained by subtracting these two measurement values:

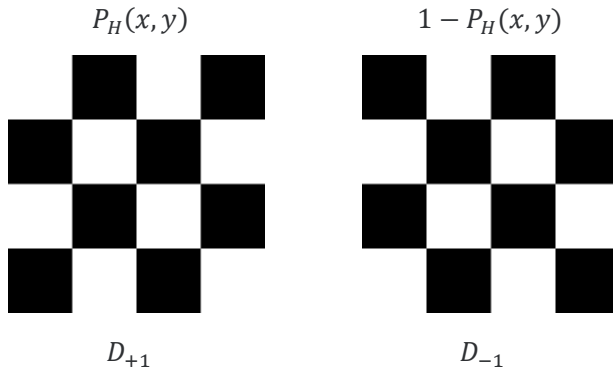


Fig. 1. Hadamard basis pattern

$$H(u, v) = D_{+1} - D_{-1} \quad (2)$$

where  $D_{+1}$  and  $D_{-1}$  correspond to  $P_H(x, y)$  and  $1 - P_H(x, y)$ , and then the image is reconstructed according to the Hadamard basis pattern and the measured coefficient correspondingly.

## 2.2. Hadamard pattern sequence optimization method: EAHSI

In traditional computational ghost imaging (CGI), a large number of patterns are required to

obtain high-quality images. However, the large number of measurements are time-consuming and not suitable for high-efficiency imaging. At present, various algorithms have been developed to reduce the number of measurements [32-34], which have the advantages of fewer measurements, short imaging time, fast imaging speed and good imaging quality. Among them, the CRHCGI [34] method is superior to other methods.

The efficiency of pattern scanning single-pixel imaging technology depends on the degree of energy concentration of the image by using the transformation [24,33]. If a transform can highly concentrate image energy in a band, that is, a small number of coefficients have large amplitude, it can simply measure these large-amplitude coefficients and ignore the rest to improve efficiency. In light of this, a novel sampling method, which is effective-area-optimized based on Hadamard single-pixel imaging technology, named EAHSI, is utilized in the sampling phase of the fast-moving object detection and tracking to achieve ultra-low sampling rate and improve the real-time performance. Compared with CRHCGI [34], our method has better performance. The contour moment is used to calculate the area of each effective region in the pattern, and the maximum value is taken, which the white is the effective region, as shown in Fig. 2. The contour of the pattern is calculated firstly, and then the area of each contour is calculated by space moment.

$$m_{ij} = \sum_{x,y} [Ctr(x, y) \cdot x^j \cdot y^i], i, j = 0, 1. \quad (3)$$

$x, y$  represents the abscissa and ordinate of the points constituting the contour  $Ctr$  in the pattern. When  $i, j$  is equal to 0, it means to calculate the contour area  $m_{00}$ .

The principle of the EAHSI: the larger the area of pattern effective region is, the more concentrated the image energy is. As a result, the Hadamard basis pattern, which can make the image energy highly concentrated, is preferentially selected to illuminate the object, and the rest is ignored. Reshaping each row (or column) of the Hadamard matrix to get the Hadamard basis pattern. The size of the Hadamard matrix is  $128^2 \times 128^2$  in our work, as illustrated in Fig. 2. The maximum area of the effective region in each pattern is reserved as the reference term of the optimized sequence, and the terms are sorted in descending order to obtain the optimized the Hadamard basis pattern sequence.

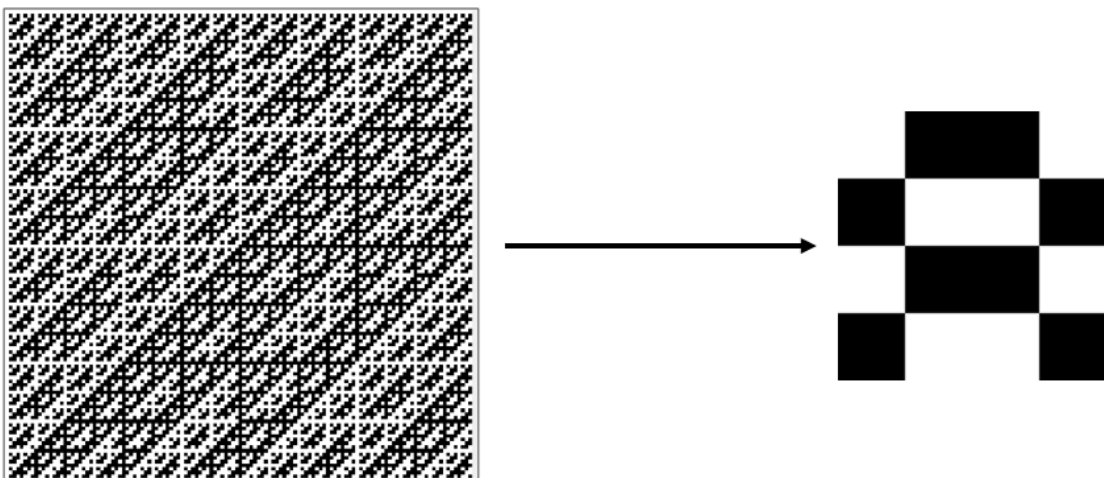


Fig. 2. The Hadamard basis pattern is obtained by reshaping the 4193rd row of the Hadamard matrix.

Our method is applied to a  $128 \times 128$  scene. When the SPI is used for full sampling, a total of 16384 patterns are required. As shown in Fig. 3, the red box in Fig. 3a marks the effective region with the largest area in the pattern, Fig. 3b is the partial pattern sequence before optimization, Fig. 3c is the partial pattern sequence after optimization. The number indicates the specific position of the pattern in the sequence.

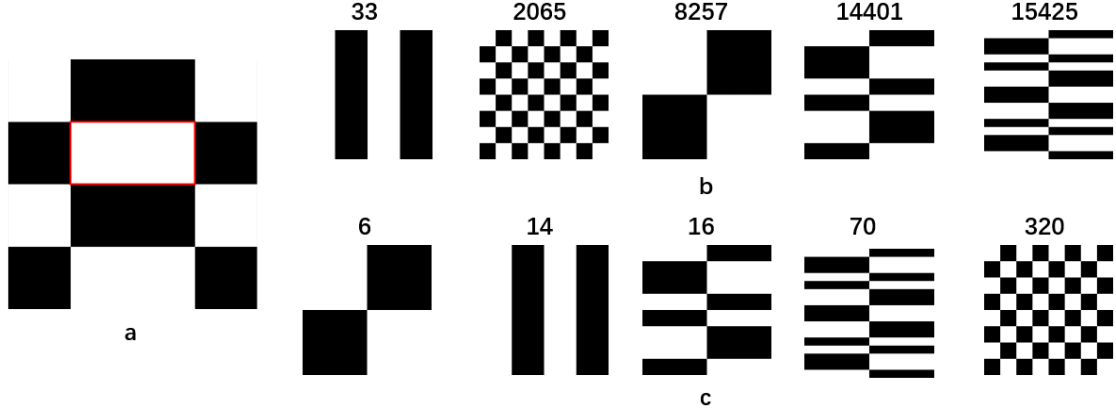


Fig. 3. The red box in 3a indicates the region with the largest effective area, the number in 3b is the position of patterns in the original sequence, and the number in 3c is the position of patterns in the optimized sequence.

Using the optimized Hadamard pattern sequence, we can collect the spectral information needed in the practical application through fewer measurement times, and then reconstruct the target. See the experimental part for details. It should be noted that the experimental imaging part is only to prove the advantage of the EAHSI, that is, to obtain better reconstruction results with fewer measurement times while it is not necessary for imaging during the detection and tracking.

### 2.3. Image-free detection and tracking method: PCGD

In this article, we propose an image-free detection and tracking method based on the PCGD, which utilizes the gradient difference of the projection curves to estimate the location of fast-moving object. Inspired by the method of Shi et al. [20], the two-dimensional image is transformed into a one-dimensional projection curve, which greatly decreases the amount of calculation and storage space. We decompose the Hadamard basis pattern to measure the Hadamard spectral more accurately and obtain more details when reconstructing the projection curve.

To improve efficiency and enhance real-time performance, we use the Hadamard basis pattern sequence optimized by the EAHSI to illuminate the fast-moving object. The pattern is decomposed into rows and columns along the x-axis and y-axis, and the sub-pattern is composed of each row and column decomposition. As shown in Fig. 4, we only use the sub-patterns that are not repeated in the composed results.

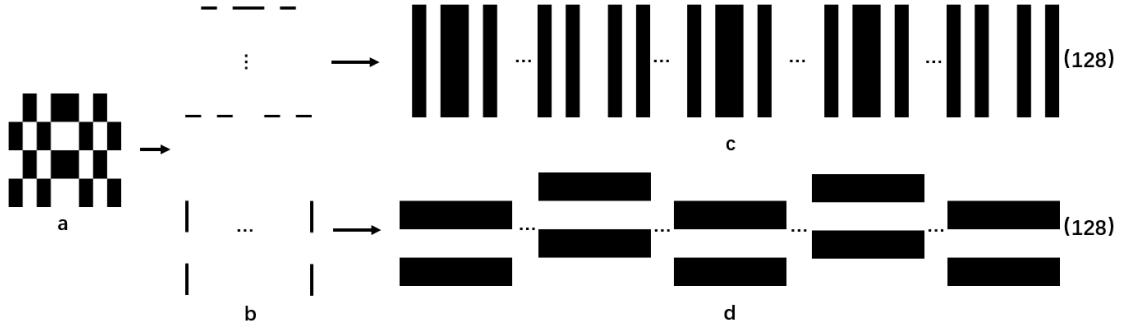


Fig. 4. The Hadamard basis pattern decomposition and the sub-patterns composition. 4a is the pattern of optimization sequence, 4b are the rows and columns decomposed from the pattern, 4c and 4d are the sub-patterns composed from the 4b.

In the whole process, it is not necessary to image the scene, but only need to apply the SPI principle to reconstruct the projection curve of the scene in the x-axis and y-axis direction, that is, to transform the two-dimensional information into one-dimensional information. And, to reduce the amount of computation, we have established a prior projection curve for the scene before the fast-moving object enters and the first-order gradient of the projection curve in the x-axis and y-axis directions.

The principle of the PCGD is as follows: First, starting from the fast-moving object entering the scene, the SPI principle is used to reconstruct the projection curve along the x-axis and y-axis. The second step is to calculate the first-order gradient of the scene projection curve. The third step is to perform a gradient difference operation on the first-order gradient of the projection curve between the scene and prior knowledge database. The fourth step is to extract the first two maximum values of the gradient difference result to obtain the position coordinates of the object in the scene. The interaction between sub-patterns and target scene is mathematically expressed as the internal product of both:

$$IP(P, I) = \sum_{x=1}^{128} \sum_{y=1}^{128} \text{abs}\{P(x, y)I(x, y)\} \quad (2)$$

where  $P$  is the sub-patterns,  $I$  is the scene,  $x$  and  $y$  are the coordinate values of the sub-patterns and the scene, and the measured value  $IP$  is collected by the single-pixel detector.

$$PC_x(m) = \sum_{x=1}^{128} P(x, m), m = 1, 2, \dots, 128. \quad (4)$$

$$PC_y(n) = \sum_{y=1}^{128} P(n, y), n = 1, 2, \dots, 128. \quad (5)$$

$$C(i) = PC(i), i = 1, 2, \dots, 128. \quad (6)$$

The  $PC_x$  and  $PC_y$ , a  $1 \times 128$  vector, represents the projection of the  $P$  along with the x-axis and y-axis. The projection curve reconstructed from the projection of sub-patterns and the measured value can be expressed as:

$$F(i) = IP(P, I) * C(i), i = 1, 2, \dots, 128. \quad (7)$$

where  $F$  is a  $1 \times 128$  one-dimensional vector, which represents the projection curve. And then, calculating the first-order gradient  $F'$  of  $F$ , that is, subtract the previous value from the next value

in the one-dimensional vector:

$$F'(i) = \nabla[F(i)] \quad (8)$$

$$F'_O(i) = \nabla[F_O(i)], \quad F'_M(i) = \nabla[F_M(i)] \quad (9)$$

$$Diff[m(i), n(i)] = abs[m(i) - n(i)], i = 1, 2, \dots, 128. \quad (10)$$

$$D(\nabla) = Diff(F'_O, F'_M) \quad (11)$$

the  $F'_O$  is the first-order gradient of the scene projection curve before the fast-moving object entered, call the prior projection curve.  $F'_M$  is the first-order gradient of the scene projection curve after the fast-moving object entered, and  $Diff$  is the gradient difference operation.

Finally, the position information of the target is obtained after the gradient difference operation.

$$(V_1, V_2) = S_2\{D(\nabla)_{Value}\} \quad (12)$$

$S_2$  means to select the first two largest values from  $D$ .

### 3. Experiment results and analysis

#### 3.1. Schematic diagram of the optical system

We demonstrate through experiment to prove that the PCCG and EAHSI methods are effective. As show in Fig. 5, the illumination system consists of a white LED, a DMD (Taxes Instruments DLP Discovery 4000 development kit), a single-pixel detector (Thorlabs DET100A2 320nm-1100nm), a data acquisition board (National Instruments USB-6343) and the projection lens.

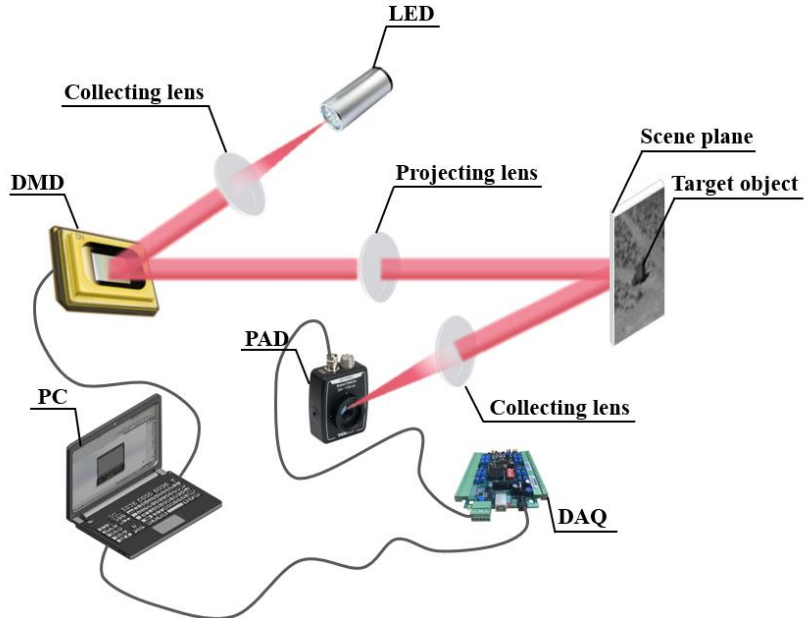


Fig. 5. Experimental set-up and Schematic diagram of the optical system.

In the illumination system, the LED is used to illuminate the DMD that has  $2560 \times 1600$  micromirrors and the pixel size is 7.6um, and the DMD is operated at a refresh rate of 22kHz. The Hadamard basis pattern displayed on DMD is projected onto the surface of the scene plane through the lens. The single-pixel detector collects the light intensity, and the data acquisition board convert the light intensity signal into a digital signal that can be processed by a computer.

### 3.2. Analysis of EAHSI sampling method

The experiment was divided into two stages. First, verify the effectiveness of EAHSI. Compared with other methods, ERHSI can reconstruct better results with fewer measurements. Without losing generality, we used both "Butterfly" and "Girl" images in the test. Fig. 6 shows the comparison between EAHSI and CRHCGI [34] when reconstructing, using the peak signal-to-noise ratio (PSNR) as the reference standard to evaluate image quality.

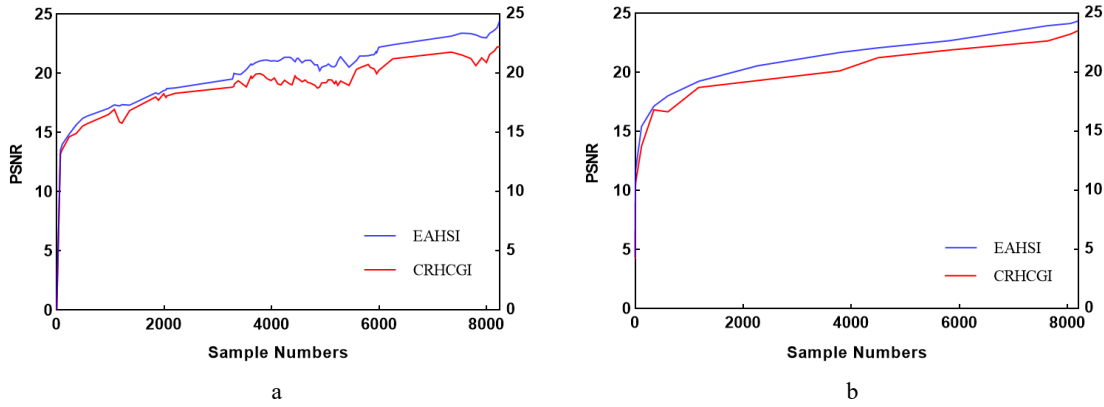


Fig. 6. The 6a and 6b are the PSNR curves of Butterfly and Girl, respectively.

It turns out to be the case that the PSNR of the EAHSI reconstruction image is higher than that of CRHCGI under the same measurement times, and the measurement times of EAHSI is much less than that of CRHCGI under the same PSNR. Therefore, the efficiency of EAHSI is higher than that of CRHCGI under the condition of obtaining the same quality reconstruction results. Fig. 7 shows the reconstructed images at different sampling rates and Table 1 lists the PSNR correspondingly. From the experimental results, it can be intuitively seen that EAHSI is better than CRHCGI.

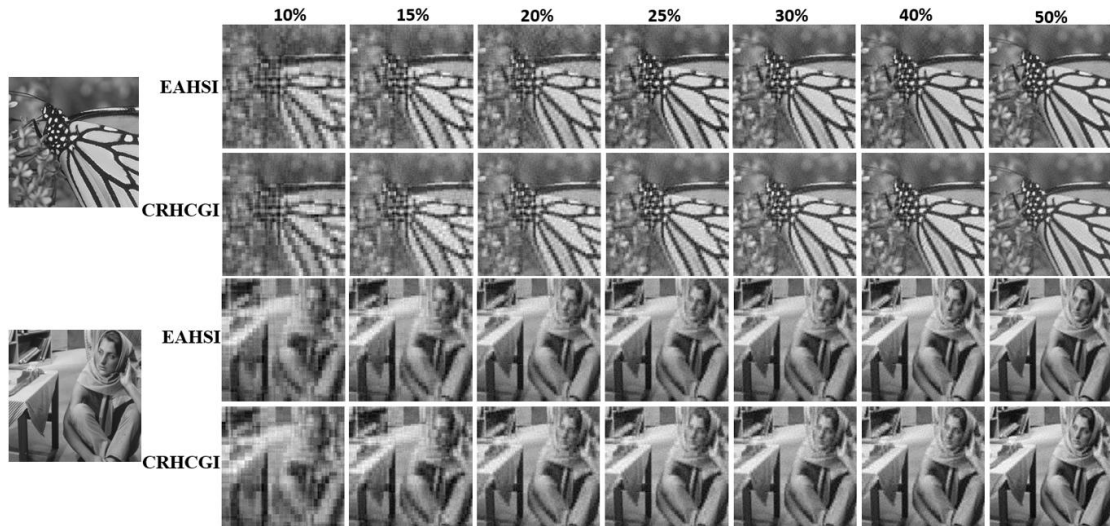


Fig. 7. Butterfly and Girl images reconstructed at different sampling rates.

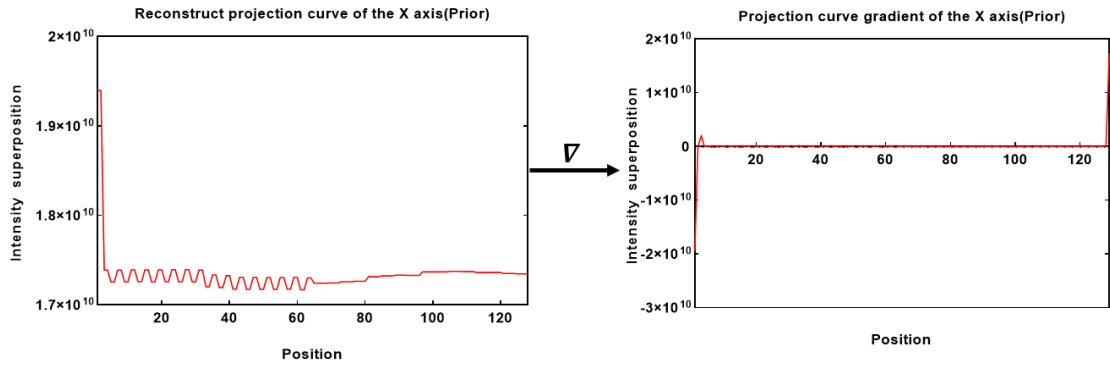
Table 1. PSNR of Butterfly and Girl at different sampling rates

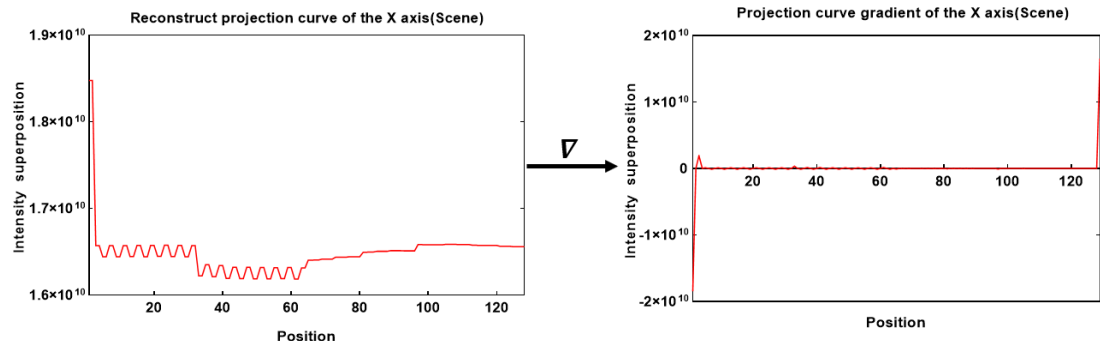
Sample	Butterfly		Girl		
	Method	EAHSI	CRHCGI	EAHSI	CRHCGI
10%		17.984	17.785	19.224	18.686
15%		18.784	17.856	20.525	20.273
20%		19.415	18.887	21.683	20.941
25%		20.973	19.406	22.026	21.338
30%		20.344	19.129	22.196	21.288
40%		22.854	22.545	22.538	21.972
50%		23.811	22.862	24.189	23.307

### 3.3. Analysis of PCGD detection and tracking method

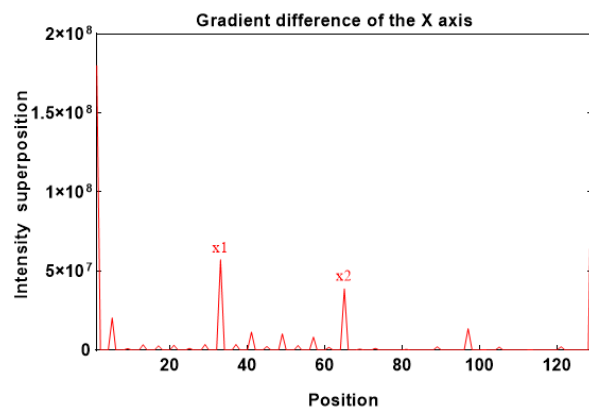
In the target detection and tracking stage, the Hadamard basis pattern sequence optimized by EAHSI is used for measurement and the light intensity signal collected by the single-pixel detector. The sub-patterns are obtained by decomposing Hadamard basis patterns and projected by DMD. And then, based on the SPI principle, the sub-patterns projection curves and the collected measurement values are used to reconstruct the position information curves. And then the gradient difference operation is further applied. Finally, the coordinate information of the fast-moving object in the complex scene is obtained.

To explain the principle of the PCGD method in detail, we show the calculation of the position information of a fast-moving object in a certain transient state in the scene. The x-axis projection curve of the scene shown on the left side of Fig. 8b is reconstructed from the x-axis projection of the sub-pattern and the single-pixel measurement value. And then the first-order gradient curve is calculated, as shown on the right side of Fig. 8b. The  $\nabla$  represents the gradient operation of a one-dimensional vector. Finally, perform a difference operation on the first-order gradient curve of the scene and the prior projection curve shown in Fig. 8a to obtain the position information in the x-axis direction, as shown in Fig. 8c. In the same way, we can obtain the position information in the direction of the y-axis, as shown in Fig. 9c. Eventually, the key position information of the fast-moving object in the scene is obtained, that is,  $(V_{1x}, V_{2x}) = (x_1, x_2)$ ,  $(V_{1y}, V_{2y}) = (y_1, y_2)$ .



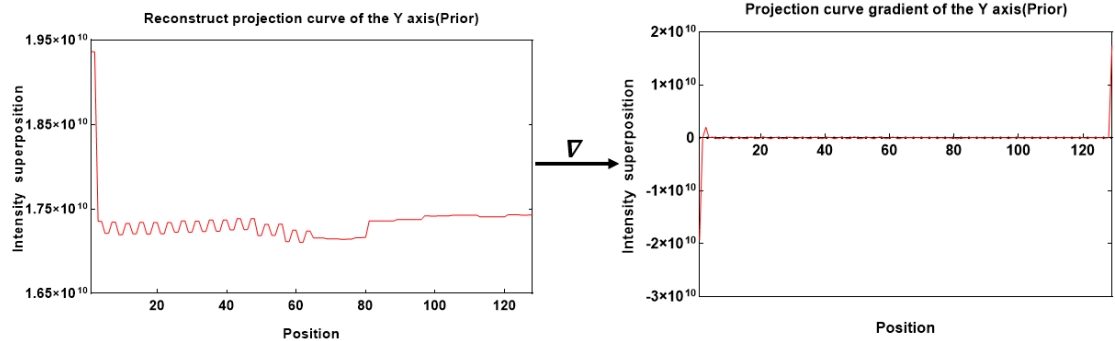


b

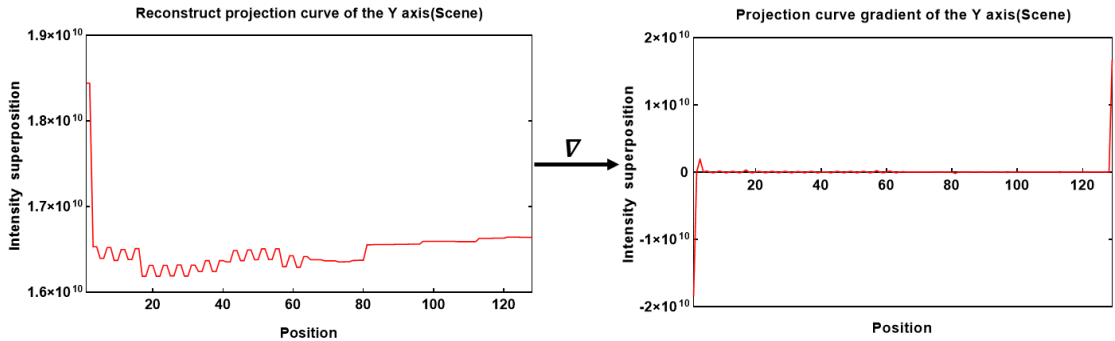


c

Fig. 8. The position information of the target in the direction of x-axis.



a



b

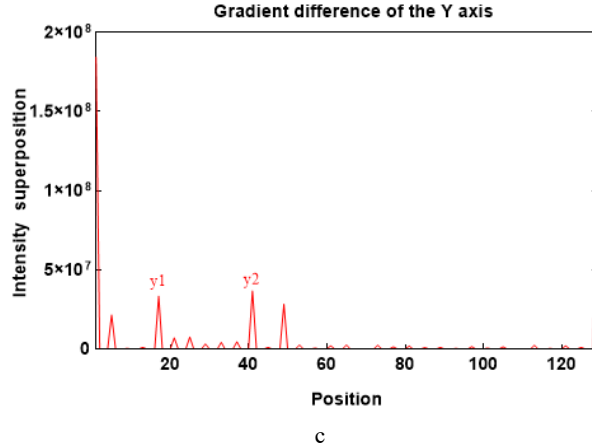
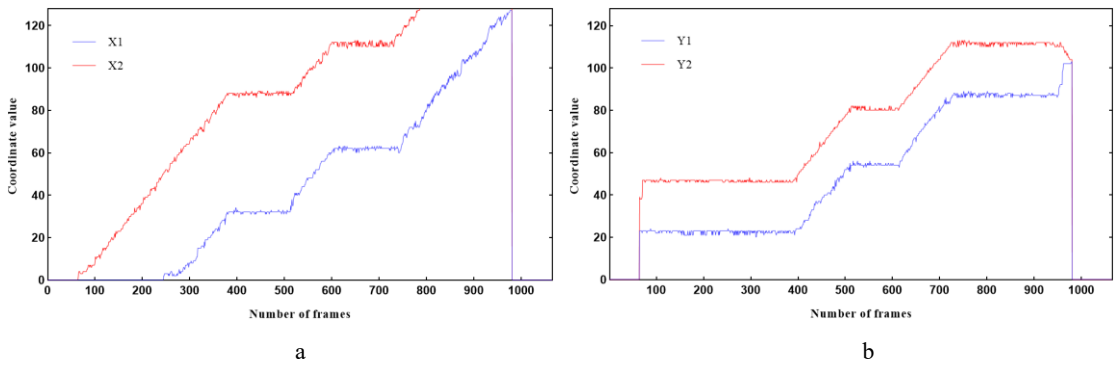


Fig. 9. The position information of the target in the direction of y-axis.

During the experiment, the data acquisition board works at the maximum sampling rate, that is, 500000 data is sampled per second, which is far higher than the refresh rate of the DMD. As a result, we take ten single-pixel measurement values for each lighting mode, average them, and then reconstruct the projection curve. The gradient difference algorithm is employed to estimate the position information contained in the projection curve. Finally, we get the position information of the object.

As shown in Fig. 10, it represents the location information corresponding to different transient states of the object in the whole moving process, that is, each frame corresponds to one position information. The horizontal axis represents the number of frames, and the vertical axis represents the coordinate values. Fig. 10a are the abscissas  $x_1$  and  $x_2$  of the target in the dynamic scene, and Fig. 10b are the ordinates  $y_1$  and  $y_2$  of the object.

In our experiment, the system does not detect the boundary information of the target before the target enters the scene. When the target enters the scene, the two boundaries in the y-axis direction can be detected at the same time, while the x-axis direction only detects  $x_2$ . When the target fully enters the scene,  $x_1$  is detected. When the  $x_2$  value reaches its maximum value, it indicates that the target is leaving the scene. When all boundary values are zero, the target is leaving the scene. We calculate the centroid of the fast-moving object in the scene through the boundary value, Figures 10c and 10d are the  $x$  and  $y$  coordinates of the centroid, respectively, and then track and detect the object.



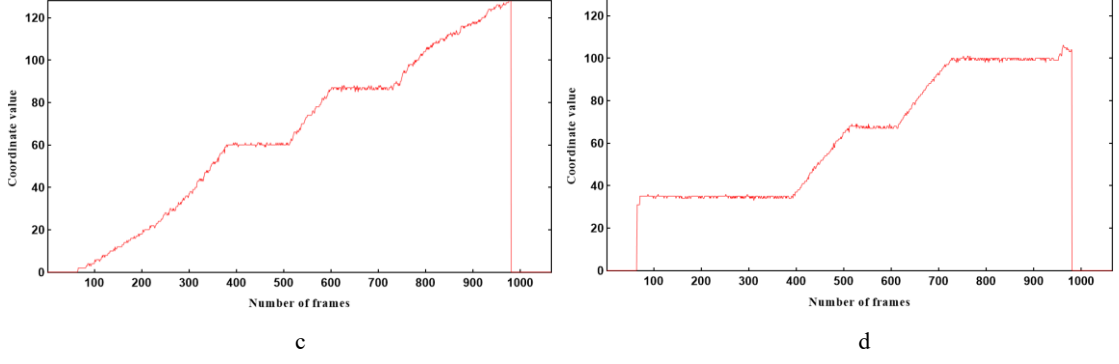


Fig. 10. Position information of the moving target at different transient states.

Our method achieves a 1.28% sampling rate, 0.00955s time resolution and 105 fps frame rate, which fully meets the requirements of real-time detection and tracking of fast-moving objects in complex scenes. In the calculation process, we need to obtain  $128 \times 2 \times 3$  intermediate data, a total of  $1024 \times 3$  bytes (about 2.9e-3MB), store 4 coordinate data, accounting for 16 bytes (about 2.45e-2MB) of location information, and the space occupied by the calculation is not more than 1MB.

Experiment results show that our strategy can not only obtain high-quality Hadamard spectral information at an ultra-low sampling rate for estimating position information, but also has the ability to ultra-low time and space consumption. Therefore, real-time target detection and tracking can be performed in a scene with complex background for a long time.

#### 4. Discussion

We have studied and analyzed the impact of high-intensity values on imaging quality and found that high-intensity values have a greater contribution to high-quality image reconstruction. The EAHSI-based methods can concentrate high-intensity values at the front end of the basis patterns strength sequence. By comparing the experimental results of EAHSI and CRHCGI, we found that EAHSI can obtain higher quality imaging at lower sampling rates.

We have found that most object detection methods are mainly used for tangential moving. By analyzing the rules of the object's axial moving, our method also may be suitable for the detection and tracking of axial moving. Combining two reference items to judge the object's moving type, and the reference item can be expressed as:

$$\mathfrak{V}_x = abs(V_{1x} - V_{2x}) \quad \mathfrak{V}_y = abs(V_{1y} - V_{2y}) \quad (15)$$

if  $\mathfrak{V}_x$  and  $\mathfrak{V}_y$  change uniformly at the same time, and the centroid is unchanged or changed slightly, it is judged to be an axial movement, and we will verify it in detail in future work.

We recognize that the method proposed has three limitations. One is that when the colour difference between the target and the scene is too small, the detection effect is poor. The other is that it can only detect and track one fast-moving object at a time. The last one is that the proposed method can only achieve two-dimensional tracking. Breaking through the above limitations is our future work.

#### 5. Conclusion

We have proposed an image-free object detection and tracking method, which combined an efficient

single-pixel measurement method to achieve real-time detection and tracking of the fast-moving object in a complex background scene. The strategy has exploited the EAHSI to reduce the number of measurements and improved the real-time performance of the system, and then used the SPI and PCGD to estimate the position information of the fast-moving object. Our method has achieved a 1.28% sampling rate, 0.00955s time resolution and 105fps frame rate, which is suitable for real-time and long-time fast-moving object detection and tracking. Benefit from the wide spectral response advantages of the single-pixel detector, our strategy can work in the invisible band to detect and track the hidden fast-moving object in real-time.

## References

- [1] S. T. Park, J. G. Lee, An efficient filtering algorithm for improved radar tracking (1996).
- [2] Chaw.Bing, Chang, Tabaczynski, J., Application of state estimation to target tracking, *Automatic Control IEEE Transactions on* (1984).
- [3] F. Daum, R. Fitzgerald, Decoupled kalman filters for phased array radar tracking, *IEEE Transactions on Automatic Control* 28 (1984) 269–283.
- [4] S. T. Park, J. G. Lee, Improved kalman filter design for three-dimensional radar tracking, *IEEE Transactions on Aerospace and Electronic Systems* 37 (2001) 727–739.
- [5] M. S. Wei, F. Xing, Z. You, A real-time detection and positioning method for small and weak targets using a 1d morphology-based approach in 2d images, *Light: Science and Application (English version)* 7 (2018) 97–106.
- [6] D. Comaniciu, V. Ramesh, P. Meer, Kernel-based object tracking, *IEEE Transactions on Pattern Analysis and Machine Intelligence* 25 (2003) 564–577.
- [7] W. Zhong, H. Lu, M.-H. Yang, Robust object tracking via sparsity-based collaborative model, *IEEE Conference on Computer Vision and Pattern Recognition* (2012).
- [8] W. Gong, C. Zhao, H. Yu, M. Chen, W. Xu, S. Han, Three-dimensional ghost imaging lidar via sparsity constraint, *Scientific Reports* 6 (2016) 26133.
- [9] L. Hu, X. Jin, G. Zeng, Lensless ghost imaging for moving objects, *Optical Engineering* 50 (2011) 7005.
- [10] Z. H. Xu, W. Chen, P. José, P. Miles, M. J. Sun, 1000 fps computational ghost imaging using led-based structured illumination, *Optics Express* 26 (2018) 2427–2434.
- [11] F. Ferri, D. Magatti, L. A. Lugiato, A. Gatti, Differential ghost imaging, *Physical review letters* 104 (2010) 253603.
- [12] B. Sun, S. S. Welsh, M. P. Edgar, J. H. Shapiro, M. J. Padgett, Normalized ghost imaging, *Optics Express* 20 (2012) 16892–16901.
- [13] W. Gong, S. Han, A method to improve the visibility of ghost images obtained by thermal light, *Physics Letters A* 374 (2010) 1005–1008.
- [14] L. Bian, J. Suo, Q. Dai, C. Feng, Experimental comparison of single-pixel imaging algorithms, *Journal of the Optical Society of America A* 35 (2017) 78.
- [15] K. Guo, S. Jiang, G. Zheng, Multilayer fluorescence imaging on a single-pixel detector, *Biomedical Optics Express* 7 (2016) 2425.
- [16] E. Li, Z. Bo, M. Chen, W. Gong, S. Han, Ghost imaging of a moving target with an unknown constant speed, *Applied Physics Letters* 104 (2014) 251120–251120–3.
- [17] X. Li, C. Deng, M. Chen, W. Gong, S. Han, Ghost imaging for an axially moving target with

an unknown constant speed, *Photonics Research* 3 (2015) 153.

- [18] S. Jiao, M. Sun, Y. Gao, T. Lei, Z. Xie, X. Yuan, Motion estimation and quality enhancement for a single image in dynamic single-pixel imaging, *Optics express* 27 (2019) 12841–12854.
- [19] Shuai, Sun, Jun-Hao, Hui-Zu, Lin, Liang, Jiang, Wei-Tao, Liu, Gradual ghost imaging of moving objects by tracking based on cross correlation., *Optics letters* 44 (2019) 5594–5597.
- [20] D. Shi, K. Yin, J. Huang, K. Yuan, W. Zhu, C. Xie, D. Liu, Y. Wang, Fast tracking of moving objects using single-pixel imaging, *Optics Communications* 440 (2019) 155–162.
- [21] Z. Zhang, X. Wang, G. Zheng, J. Zhong, Image-free real-time detection and tracking of fast moving object using a single-pixel detector., *Optics express* 27 (2019) 35394–35401.
- [22] M. P. Edgar, G. M. Gibson, M. J. Padgett, Principles and prospects for single-pixel imaging, *Nature Photonics* 13 (2019) 13–20.
- [23] Z. Zhang, X. Ma, J. Zhong, Single-pixel imaging by means of fourier spectrum acquisition, *Nature Communications* 6 (2014) 6225.
- [24] Z. Zhang, X. Wang, G. Zheng, J. Zhong, Hadamard single-pixel imaging versus fourier single-pixel imaging, *Optics Express* 25 (2017) 19619–19639.
- [25] Z. Zhang, S. Liu, J. Peng, M. Yao, G. Zheng, J. Zhong, Simultaneous spatial, spectral, and 3d compressive imaging via efficient fourier single-pixel measurements, *Optica* 5 (2018) 315–319.
- [26] M. Sun, M. P. Edgar, G. M. Gibson, B. Sun, N. Radwell, R. Lamb, M. J. Padgett, Single-pixel three-dimensional imaging with time-based depth resolution, *Nature Communications* 7 (2016) 12010.
- [27] W. K. Pratt, J. Kane, H. C. Andrews, Hadamard transform image coding, *Proceedings of the IEEE* 57 (1969) 58–68.
- [28] Decker, Jr, A. J., Hadamard-transform image scanning, *Applied Optics* 9 (1970) 1392–1395.
- [29] J. Gourlay, P. Mcowan, D. G. Vass, I. Underwood, M. Worboys, Time-multiplexed optical hadamard image transforms with ferroelectric-liquid-crystal-over-silicon spatial light modulators, *Optics Letters* 18 (1993) 1745–7.
- [30] C. M. Watts, D. Shrekenhamer, J. Montoya, G. Lipworth, J. Hunt, T. Sleasman, S. Krishna, D. R. Smith, W. J. Padilla, Terahertz compressive imaging with metamaterial spatial light modulators, *Nature Photonics* 8 (2014) 605–609.
- [31] M.-J. Sun, M. P. Edgar, D. B. Phillips, G. M. Gibson, M. J. Padgett, Improving the signal-to-noise ratio of single-pixel imaging using digital microscanning, *Optics Express* 24 (2016) 10476–10485.
- [32] X. Yu, R. I. Stantchev, F. Yang, E. Pickwell-MacPherson, Super sub-nyquist singlepixel imaging by total variation ascending ordering of the hadamard basis, *Scientific Reports* 10 (2020) 9338.
- [33] M.-J. Sun, L.-T. Meng, M. P. Edgar, M. J. Padgett, N. Radwell, A russian dolls ordering of the hadamard basis for compressive single-pixel imaging, *Scientific Reports* 7 (2017) 3464.
- [34] H. Wu, G. Zhao, R. Wang, H. Xiao, D. Wang, J. Liang, L. Cheng, R. Liang, Computational ghost imaging system with 4-connected-region-optimized Hadamard pattern sequence, *Optics and Lasers in Engineering* 132 (2020) 106105.